fortune Journals

Research Article

JOURNAL OF RADIOLOGY AND CLINICAL IMAGING

ISSN: 2644-2809

Gadoxetic Acid–Enhanced T1 Mapping Enables Transporter-Mediated Molecular Imaging of Liver Functional Reserve

Yuting Zhu[1‡], Xun Hu[1‡], Zhuo Shi[1], Yuan Liang[1], Dengfeng Li[1], Peiqing Ma[2], Dong Yan[3], Jianwei Liang[4], Qian Wang[1*]

Abstract

Aim: To establish a quantitative transporter-mediated imaging framework based on gadoxetic acid–enhanced T1 mapping and evaluate the relative change in longitudinal relaxation rate (ΔR1%) as an imaging biomarker of liver functional reserve (LFR).

Methods: Experimental liver injury models representing transporter deficiency, fibrosis, metabolic steatohepatitis, and alcohol-associated fatty liver disease were evaluated using serial hepatobiliary T1 mapping following Gd-EOB-DTPA administration. ΔR1% was calculated to characterize hepatobiliary enhancement kinetics. Liver functional reserve was independently assessed using multispectral optoacoustic imaging of indocyanine green (ICG) pharmacokinetics and serum ICG retention assays. Histological and transporter expression analyses were performed for mechanistic interpretation.

Results: ΔR1% mapping demonstrated distinct model-dependent hepatobiliary enhancement patterns. The transporter-deficient knockout model exhibited minimal enhancement, whereas fibrosis and steatotic injury models showed intermediate but distinguishable functional alterations. Mixed-effects analysis demonstrated significant effects of time, group, and time × group interaction on ΔR1% dynamics (all $P < 0.0001$). MRI-derived ΔR1% parameters showed no significant correlation with optoacoustic kinetic metrics but demonstrated a strong inverse correlation with serum ICG retention at 600 s ($r = -0.729$, $P < 0.0001$). Histological and molecular analyses revealed heterogeneous fibrosis, steatosis, and transporter expression among models. Notably, Oatp1b2 and Mrp2 expression levels did not parallel imaging-derived functional measurements.

Conclusion: Quantitative ΔR1% mapping derived from Gd-EOB-DTPA–enhanced T1 mapping provides a transporter-mediated imaging biomarker reflecting integrated hepatobiliary transport function across heterogeneous liver injury states. This approach offers a mechanistically grounded and potentially translatable strategy for noninvasive assessment of liver functional reserve.

Keywords: Quantitative hepatobiliary MRI; Gd-EOB-DTPA; T1 mapping; Liver functional reserve; Functional MRI; Indocyanine green; Transporter-mediated imaging

Abbreviations

Gd-EOB-DTPA –Gadolinium ethoxybenzyl diethylenetriamine pentaacetic acid (gadoxetate disodium), a hepatocyte-specific magnetic resonance imaging (MRI) contrast agent.

Affiliation:

[1]Department of Imaging Diagnosis, National Cancer Center/National Clinical Research Center for Cancer/Cancer Hospital, Chinese Academy of Medical Sciences and Peking Union Medical College, Beijing, China

[2]Department of Pathology, National Cancer Center/National Clinical Research Center for Cancer/Cancer Hospital, Chinese Academy of Medical Sciences and Peking Union Medical College, Beijing, China

[3]Department of Interventional Therapy, National Cancer Center/National Clinical Research Center for Cancer/Cancer Hospital, Chinese Academy of Medical Sciences and Peking Union Medical College, Beijing, China

[4]Department of Colorectal Surgery, National Cancer Center/National Clinical Research Center for Cancer/Cancer Hospital, Chinese Academy of Medical Sciences and Peking Union Medical College, Beijing, China

‡These authors contributed equally to this work.

Corresponding author:
Qian Wang, Department of Imaging Diagnosis, National Cancer Center/National Clinical Research Center for Cancer/Cancer Hospital, Chinese Academy of Medical Sciences and Peking Union Medical College, Beijing, China

Citation: Yuting Zhu, Xun Hu, Zhuo Shi, Yuan Liang, Dengfeng Li, Peiqing Ma, Dong Yan, Jianwei Liang, Qian Wang. Gadoxetic Acid–Enhanced T1 Mapping Enables Transporter-Mediated Molecular Imaging of Liver Functional Reserve Journal of Radiology and Clinical Imaging. 9 (2026): 78-88.

Received: May 16, 2026
Accepted: May 19, 2026
Published: July 13, 2026

MRI – Magnetic Resonance Imaging

ΔR1% – Change in longitudinal relaxation rate (R1) before and after contrast administration

ICG – Indocyanine Green

LFR – Liver Functional Reserve

CCl_4 – Carbon Tetrachloride (used to induce liver fibrosis)

MCD – Methionine-Choline Deficient diet (model of non-alcoholic steatohepatitis)

AFLD – Alcoholic Fatty Liver Disease (Lieber-DeCarli diet model)

KO – Knockout (Slco1b2/Slco1a5 double-knockout mice)

Oatp – Organic anion transporting polypeptides; murine orthologs of human OATP transporters.

Mrp – Multidrug resistance–associated proteins, key hepatocellular efflux transporters.

pCLE – Probe-based Confocal Laser Endomicroscopy

qRT-PCR – Quantitative Reverse-Transcription Polymerase Chain Reaction (qRT-PCR)

ANOVA – Analysis of Variance

SD – Standard Deviation

Introduction

Chronic liver disease (CLD) represents a major global health burden [1] and is characterized by progressive deterioration of liver functional reserve (LFR), ultimately leading to cirrhosis, hepatic decompensation, and hepatocellular carcinoma [2,3]. Reliable and quantitative assessment of LFR is therefore essential for disease stratification, prognostic evaluation, perioperative risk assessment, and therapeutic decision-making. From a physiological perspective, LFR reflects the integrated capacity of hepatocytes to coordinate substrate uptake, intracellular metabolism, and biliary excretion across the hepatobiliary transport network [4-6]. Current clinical assessment of liver function relies primarily on composite clinical scoring systems, such as the Child–Pugh classification, and systemic clearance assays including indocyanine green (ICG) retention testing [7]. Although widely used, these approaches possess important limitations. Clinical scoring systems incorporate subjective variables and may lack sensitivity to early functional impairment, whereas serum ICG-based assays require invasive sampling and provide only a global estimate of hepatic clearance without spatial information or mechanistic specificity [8,9]. Consequently, there remains a substantial unmet need for quantitative imaging approaches capable of noninvasively interrogating hepatocellular transport function at the whole-organ level. Hepatocyte-specific magnetic resonance imaging (MRI) contrast agents provide a unique opportunity to bridge molecular transport activity and organ-level functional imaging. Gadolinium ethoxybenzyl diethylenetriamine pentaacetic acid (Gd-EOB-DTPA) undergoes hepatocellular uptake predominantly through organic anion-transporting polypeptides (Oatps), followed by biliary excretion mediated by multidrug resistance–associated proteins (Mrps) [10-13]. Because this hepatobiliary handling pathway is intrinsically transporter-dependent, the resulting enhancement pattern provides a physiologically relevant imaging surrogate of hepatocellular transport activity and liver functional reserve [14-19]. In current clinical and experimental practice, Gd-EOB-DTPA–enhanced MRI is commonly interpreted using relative signal intensity–based metrics [20]. However, signal intensity measurements are intrinsically influenced by acquisition parameters, receiver gain, field strength, and scanner-dependent scaling, thereby limiting reproducibility and interstudy comparability [21]. Quantitative T1 mapping addresses these limitations by directly measuring intrinsic tissue relaxation properties independent of arbitrary signal scaling [22,23]. When combined with hepatocyte-specific contrast agents, quantitative T1 mapping enables calculation of the relative change in longitudinal relaxation rate (ΔR1%), a physically defined and standardized imaging parameter reflecting tissue-level accumulation and clearance of hepatobiliary contrast agents [24,25].

Despite increasing interest in quantitative hepatobiliary MRI [26,27], interpretation of transporter-mediated enhancement remains incompletely understood in chronic liver disease. Hepatobiliary transport processes are dynamically altered across different pathological conditions, including steatohepatitis, fibrosis, alcohol-associated liver injury, and genetic transporter deficiency [28-32]. Importantly, these disease states may differentially affect hepatocellular uptake and excretion pathways, creating substantial inter-model heterogeneity in transporter expression and function. Whether a single MRI-derived parameter such as ΔR1% can robustly reflect integrated liver functional reserve across heterogeneous disease conditions therefore remains an unresolved question. Moreover, the relationship between transporter abundance and imaging-derived functional readouts may not be linear. Hepatic contrast handling represents the integrated output of coordinated transporter activity, perfusion, intracellular processing, canalicular excretion, and microstructural integrity rather than the isolated expression level of any individual transporter. Consequently, imaging-derived enhancement metrics may better reflect systems-level hepatobiliary function than static molecular measurements alone. To address these questions, the present study systematically evaluated Gd-EOB-DTPA–enhanced quantitative T1 mapping across multiple experimental liver injury models with distinct pathophysiological mechanisms, including methionine–choline-deficient (MCD) diet–induced steatohepatitis, alcohol-associated fatty liver disease (AFLD), carbon tetrachloride (CCl_4)–induced fibrosis, and

a transporter-deficient Slco1b2/Slco1a5 double-knockout model serving as a functional reference. Quantitative ΔR1% kinetics were integrated with independent assessment of liver functional reserve using serum ICG retention assays and multispectral optoacoustic imaging of hepatic ICG pharmacokinetics. Histological and molecular analyses of hepatocellular transporters were further performed to support mechanistic interpretation. We hypothesized that ΔR1% reflects the integrated systems-level functional output of hepatobiliary transport processes rather than the isolated abundance of individual transporters. Establishing such a transporter-mediated quantitative imaging biomarker would support the translational application of Gd-EOB-DTPA–enhanced T1 mapping as a standardized and mechanistically meaningful approach for noninvasive assessment of liver functional reserve.

Methods

Animal Models

Female wild-type C57BL/6J mice (6–8 weeks old; Beijing Vital River Laboratory Animal Technology Co., Ltd., China) were housed under controlled environmental conditions (22 ± 2 °C, 50–60% humidity, 12 h light/dark cycle) with free access to food and water. Sample size (n = 6 per group) was determined according to previous small-animal imaging studies to ensure adequate statistical power for longitudinal and intergroup comparisons. Animals were randomly assigned using a computer-generated randomization scheme into the following groups: control, carbon tetrachloride (CCl_4)-induced fibrosis, methionine–choline-deficient (MCD) diet–induced steatohepatitis, and alcohol-associated fatty liver disease (AFLD). Fibrosis was induced by intraperitoneal injection of 10% (v/v) CCl_4 diluted in olive oil (10 μL/g body weight) every 3 days for 6 weeks. MCD-induced steatohepatitis was established by ad libitum feeding with an MCD diet (TP3622, Nantong TeloPharm, China) for 6 weeks. AFLD was induced using a Lieber–DeCarli liquid diet (TP4030B, Nantong TeloPharm; 4% ethanol, ~28% caloric contribution) for 6 weeks. All procedures were performed at matched circadian time points. Slco1b2/Slco1a5 double-knockout (KO) mice (C57BL/6J background; Shanghai Model Organisms Center, Inc., China) were included as a transporter-deficient reference model. Genotypes were confirmed by PCR before inclusion. Detailed genotyping procedures and validation data are provided in the Supporting Information (Section 1, Table S1, Figure S1). All experimental procedures were approved by the Ethics Committee for Laboratory Animals of the Cancer Hospital, Chinese Academy of Medical Sciences (Approval No. NCC2022A571) and complied with ARRIVE guidelines.

MRI Acquisition and ΔR1% Analysis

MRI examinations were performed using a 9.4 T small-animal imaging system (Bruker BioSpec, Ettlingen, Germany) equipped with a 26-mm volume coil. Mice were anesthetized with 1.5–2.0% isoflurane in oxygen. Body temperature (37.0 ± 0.5 °C) and respiratory rate were continuously monitored throughout imaging. Respiratory gating was applied during all acquisitions. A 26G tail vein catheter was inserted for contrast administration. Gd-EOB-DTPA (Primovist®, Bayer Healthcare) was intravenously administered at 0.025 mmol/kg (~50 μL), followed by a 100 μL saline flush. Quantitative T1 mapping was performed using a respiratory-gated variable repetition time (VTR) FLASH sequence. Multiple repetition times were acquired under identical imaging geometry with a constant excitation flip angle. T1 values were estimated using voxel-wise nonlinear fitting of the longitudinal recovery model.

Imaging parameters included a field of view of 30 × 30 mm², matrix size of 256 × 256, slice thickness of 0.5 mm, and in-plane resolution of 0.15 × 0.15 mm². Detailed imaging parameters are summarized in Supporting Information Table S2. Post-contrast T1 mapping was performed at 10, 20, 30, and 40 min after contrast administration using identical acquisition settings. Pre-contrast T1 mapping served as baseline. Regions of interest (ROIs) were manually delineated within the liver parenchyma while avoiding large vessels and bile ducts. ROI placement was performed in a blinded manner and propagated across all time points.

The longitudinal relaxation rate was calculated as: R1 = 1/T1. Relative enhancement was quantified as:

$$\Delta R1\ (t,\%) = \frac{R1_t - R1_0}{R1_0} \times 100,$$

where $R1_0$ represents the pre-contrast value and $R1_t$ represents the post-contrast value at each time point.

Optoacoustic Imaging and ICG Kinetics

Hepatic indocyanine green (ICG) kinetics were evaluated using a multispectral optoacoustic imaging system (Vevo LAZR-X, FUJIFILM VisualSonics). Following intravenous administration of ICG (1 mg/kg), dynamic imaging was continuously performed for 500 s to assess hepatic uptake and clearance kinetics. ROIs were manually delineated over the liver parenchyma, and signal enhancement was quantified relative to baseline. Longitudinal signal profiles were analyzed using a restricted maximum likelihood (REML)-based mixed-effects model with time as a repeated factor and experimental group as a fixed effect. Pharmacokinetic parameters extracted from time–signal curves included the area under the curve from 0–500 s ($AUC_{0\text{-}500}$ s), peak signal intensity (Peak Y), and time to peak enhancement (T_{max}). Because AUC and Tmax did not consistently satisfy normality assumptions, intergroup comparisons were performed using the Kruskal–Wallis test followed by Dunn's multiple-comparison correction. Peak Y was analyzed using one-way ANOVA with Tukey's post hoc correction.

Zhu Y, et al., J Radiol Clin Imaging 2026
DOI:10.26502/jrci.2809135

Serum ICG Spectrophotometric Analysis

Systemic ICG clearance was evaluated spectrophotometrically. Following intravenous administration of ICG (1 mg/kg), blood samples were collected via retro-orbital bleeding at 0 s, 300 s, and 600 s. Serum ICG concentration at 0 s was defined as the reference value (100%), and subsequent measurements were expressed as percentages of baseline. Serum ICG retention at 600 s was selected as the primary endpoint reflecting systemic clearance capacity and liver functional reserve.

Histological and Molecular Analyses

In vivo hepatic microarchitecture was evaluated using probe-based confocal laser endomicroscopy following intravenous administration of fluorescein isothiocyanate–dextran. A fiber-optic probe was positioned on the liver surface to obtain real-time images of sinusoidal architecture and microvascular perfusion. After imaging, mice were euthanized and liver tissues were harvested for histological and molecular analyses. Total RNA was extracted using TRIzol reagent, and quantitative reverse-transcription polymerase chain reaction (qRT-PCR) was performed using SYBR Green chemistry. Slco1b2 and Abcc2 expression levels were normalized to β-actin using the $2^{-\Delta\Delta Ct}$ method. For protein analysis, liver tissues were lysed in RIPA buffer, and equal amounts of protein were separated by SDS–PAGE and transferred onto membranes for immunoblotting. Primary antibodies included anti-MRP2/ABCC2 (bs-1092R, 1:1000, Bioss) and anti-Oatp4 (sc-376904, 1:1000, Santa Cruz Biotechnology), which recognizes mouse Oatp1b2. β-Actin served as the loading control. Band intensities were quantified using Image J. Molecular analyses were performed in a subset of animals (n = 3 per group). For histological evaluation, liver tissues were fixed, paraffin-embedded, sectioned, and stained with Masson's trichrome. Frozen sections were stained with Oil Red O for lipid visualization. Histological assessment was performed in a blinded manner.

Statistical Analysis

Statistical analyses were performed using GraphPad Prism (version 10.1.2). Normality was assessed using the Kolmogorov–Smirnov test. Parametric or nonparametric tests were applied as appropriate. Longitudinal data were analyzed using REML-based mixed-effects models. Intergroup comparisons were performed using one-way ANOVA or Kruskal–Wallis tests with appropriate post hoc corrections. Correlations were evaluated using Spearman rank correlation analysis. Data are presented as mean ± standard deviation (SD). A two-sided P value < 0.05 was considered statistically significant.

Safety Statement

No unexpected or unusually high safety hazards were encountered during this study.

Results

Establishment of Experimental Liver Injury Models

As summarized in Figure 1, four experimental liver injury models were successfully established in addition to normal controls and a transporter-deficient genetic reference model. These included a Slco1b2/Slco1a5 double-knockout (KO) model, a carbon tetrachloride (CCl_4)-induced fibrosis model, a methionine–choline-deficient (MCD) diet–induced metabolic injury model, and an alcohol-associated fatty liver disease (AFLD) model. Together, these models represented distinct etiologies of hepatocellular dysfunction and were subsequently evaluated using quantitative MRI, optoacoustic imaging, and ex vivo analyses.

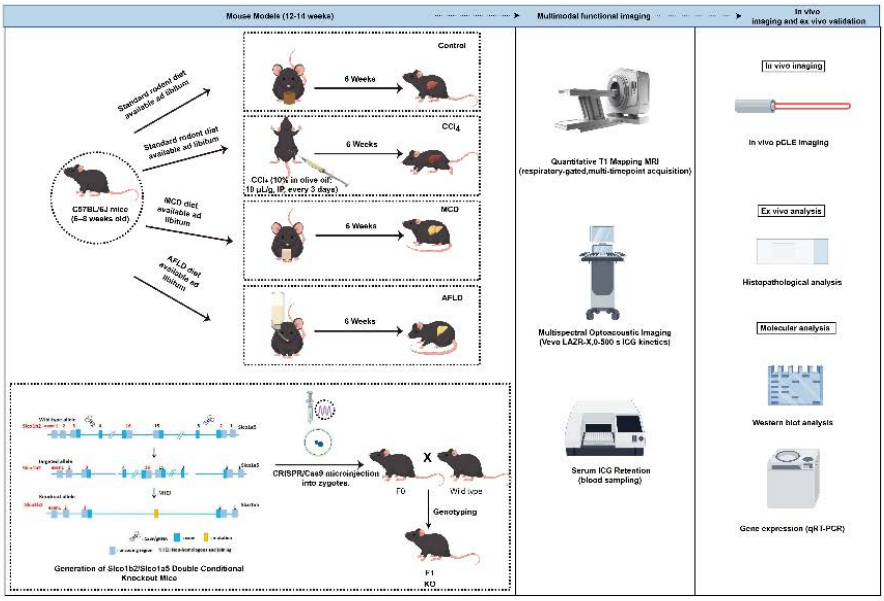

Figure 1: Schematic overview of experimental design and multimodal.

Citation: Yuting Zhu, Xun Hu, Zhuo Shi, Yuan Liang, Dengfeng Li, Peiqing Ma, Dong Yan, Jianwei Liang, Qian Wang. Gadoxetic Acid–Enhanced T1 Mapping Enables Transporter-Mediated Molecular Imaging of Liver Functional Reserve Journal of Radiology and Clinical Imaging. 9 (2026): 78-88.

Zhu Y, et al., J Radiol Clin Imaging 2026
DOI:10.26502/jrci.2809135

Evaluation framework

The schematic illustration consists of three panels. Left: establishment of experimental liver injury models, including normal control mice (Control), carbon tetrachloride–induced liver fibrosis (CCl_4), methionine–choline–deficient (MCD) diet–induced steatohepatitis, alcoholic fatty liver disease induced by a Lieber–DeCarli ethanol liquid diet (AFLD), and Slco1b2/Slco1a5 double-knockout mice (KO). Middle: in vivo functional assessment using multimodal imaging approaches, including gadolinium ethoxybenzyl diethylenetriamine pentaacetic acid (Gd-EOB-DTPA)–enhanced magnetic resonance imaging (MRI), indocyanine green (ICG) clearance, and photoacoustic (PA) imaging. Right: in vivo imaging–based and ex vivo validation analyses, including probe-based confocal laser endomicroscopy (pCLE), Western blotting, quantitative PCR (qPCR), and histopathological evaluation. Figure created with Figdraw.

Quantitative Hepatobiliary T1 Mapping Revealed Distinct Functional Enhancement Patterns

Dynamic changes in hepatic R1 and derived ΔR1% following Gd-EOB-DTPA administration demonstrated distinct model-dependent hepatobiliary enhancement kinetics (Figure 2).

(A) Representative hepatic T1 parametric maps acquired at baseline and at 10–40 min after contrast administration in each group (unit: seconds). Parametric maps were displayed using a color-coded scale with a fixed range of 0–1 s, enabling direct visual comparison across groups and time points.

(B) Longitudinal changes in hepatic ΔR1% relative to baseline following Gd-EOB-DTPA administration (mean ± SD, n = 6 per group). All groups exhibited peak enhancement at 10 min, followed by progressive washout over time. The control group demonstrated the greatest enhancement magnitude, whereas the transporter-deficient KO group showed minimal signal increase throughout the dynamic phase. The CCl_4, MCD, and AFLD models exhibited distinct intermediate enhancement kinetics, reflecting differential impairment of hepatobiliary contrast uptake and retention.

Representative T1 maps (Figure 2A) were reconstructed using a fixed color scale (0–1 s) uniformly applied across all groups and time points, enabling direct visual comparison independent of display windowing. Baseline and post-contrast T1 values are summarized in Supporting Information Table S3. Baseline hepatic T1 values were comparable among groups, whereas post-contrast reductions varied substantially, consistent with differences in hepatobiliary contrast uptake and retention. Longitudinal ΔR1% analysis using a REML-based mixed-effects model (Figure 2B) demonstrated significant effects of time, group, and time × group interaction (all $P < 0.0001$). The control group exhibited the highest cumulative enhancement and peak ΔR1%, whereas the KO group demonstrated minimal enhancement, indicating severely impaired hepatocellular uptake. The CCl_4, MCD, and AFLD groups exhibited intermediate yet clearly distinguishable enhancement patterns.

Optoacoustic Imaging Demonstrated Altered Intrahepatic ICG Pharmacokinetics

Multispectral optoacoustic imaging revealed distinct intrahepatic ICG pharmacokinetics across experimental groups (Figure 3A–B). Because the KO group demonstrated negligible hepatic signal without a discernible enhancement peak, pharmacokinetic fitting was not feasible, and subsequent analyses were restricted to the remaining groups. Mixed-effects modeling demonstrated significant effects of time, group, and time × group interaction (all $P < 0.0001$). Quantitative $AUC_{0\text{-}500\ s}$ and peak signal intensity differed significantly among groups, whereas Tmax did not reach statistical significance.

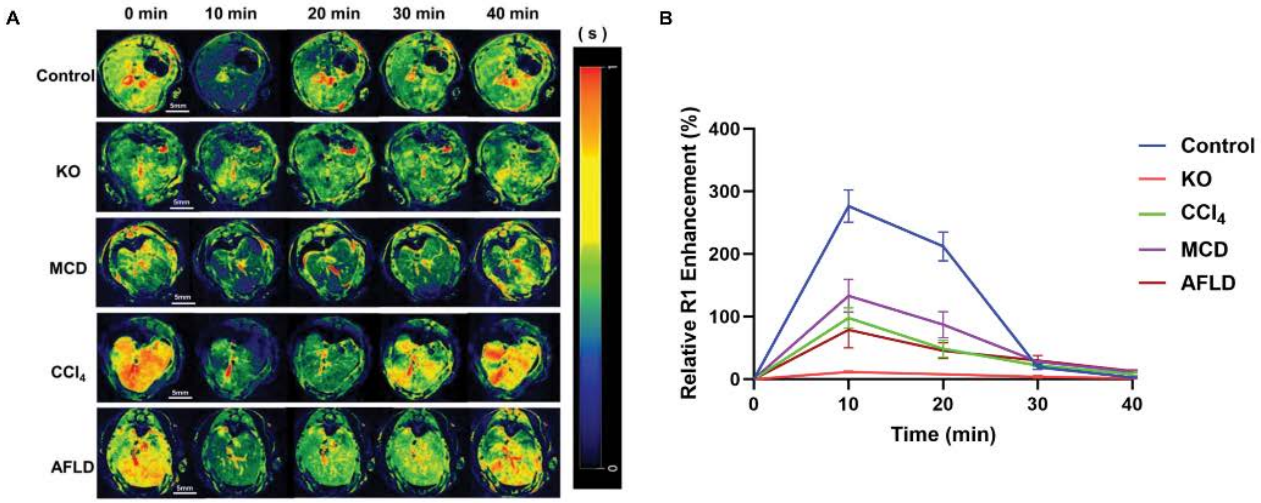

Figure 2: Hepatic T1 Dynamics and Derived ΔR1% Following Gadoxetic Acid Administration.

Citation: Yuting Zhu, Xun Hu, Zhuo Shi, Yuan Liang, Dengfeng Li, Peiqing Ma, Dong Yan, Jianwei Liang, Qian Wang. Gadoxetic Acid–Enhanced T1 Mapping Enables Transporter-Mediated Molecular Imaging of Liver Functional Reserve Journal of Radiology and Clinical Imaging. 9 (2026): 78-88.

Zhu Y, et al., J Radiol Clin Imaging 2026
DOI:10.26502/jrci.2809135

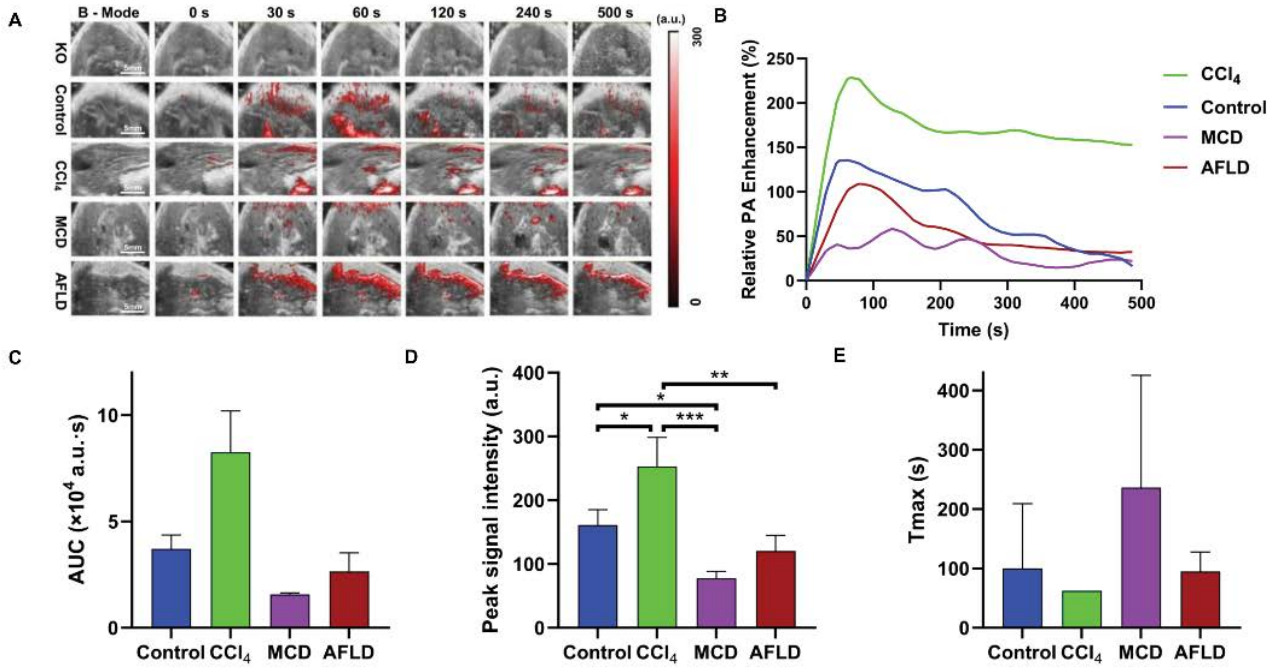

Figure 3: Hepatic indocyanine green (ICG) pharmacokinetics assessed by multispectral optoacoustic imaging.

Hepatic ICG dynamics were evaluated using a small-animal multispectral optoacoustic imaging system (Vevo LAZR-X, FUJIFILM VisualSonics).

(A) Representative optoacoustic images acquired before and after intravenous ICG administration, including B-mode reference images and dynamic images at 0, 30, 60, 120, 240, and 500 s. All images are displayed using a fixed color scale (0–300 a.u.) to ensure direct visual comparability across groups and time points. Signal intensity is visualized using a pseudocolor scale ranging from dark (minimum) to bright (maximum), with increasing intensity represented by red-dominant coloration.

(B) Real-time hepatic ICG enhancement curves over 0–500 s. Curves were smoothed using locally weighted scatterplot smoothing (LOWESS). Enhancement profiles differed significantly over time and among groups (mixed-effects model: time effect, $P < 0.0001$; group effect, $P = 0.0004$).

(C) Area under the curve ($AUC_{0–500\ s}$) of hepatic ICG enhancement.

(D) Peak signal intensity.

(E) Time to peak (T_{max}).

Data are presented as mean ± SD. The KO group was excluded from quantitative kinetic analysis due to negligible hepatic enhancement precluding reliable fitting.

MRI-Derived ΔR1% Correlated with Systemic ICG Clearance

Serum ICG retention analysis (Figure 4A) demonstrated distinct systemic clearance profiles among experimental groups. The KO group exhibited markedly impaired ICG elimination, whereas controls demonstrated near-complete clearance at 600 s. Correlation analysis revealed no significant association between MRI-derived ΔR1% parameters and optoacoustic kinetic parameters, indicating limited cross-modality concordance in quantifying intrahepatic contrast handling. In contrast, ΔR1% AUC demonstrated a strong inverse correlation with serum ICG retention at 600 s ($r = −0.729$, $P < 0.0001$), supporting its association with systemic hepatic clearance capacity.

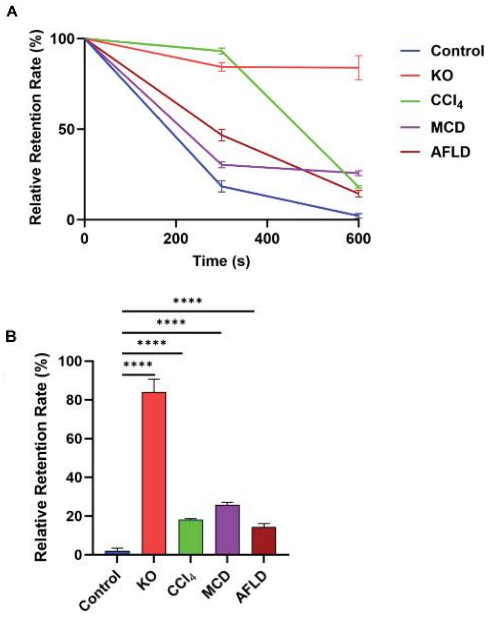

Figure 4: Serum ICG retention profiles across experimental groups.

Citation: Yuting Zhu, Xun Hu, Zhuo Shi, Yuan Liang, Dengfeng Li, Peiqing Ma, Dong Yan, Jianwei Liang, Qian Wang. Gadoxetic Acid–Enhanced T1 Mapping Enables Transporter-Mediated Molecular Imaging of Liver Functional Reserve Journal of Radiology and Clinical Imaging. 9 (2026): 78-88.

(A) Time-dependent changes in serum ICG retention following intravenous injection, expressed as a percentage of baseline (0 s).

(B) Serum ICG retention at 600 s. All non-control groups exhibited significantly higher retention than controls ($P < 0.0001$).

Data is presented as mean ± SD.

Histological and Molecular Analyses Revealed Structural and Transporter Heterogeneity

Probe-based confocal laser endomicroscopy demonstrated preserved sinusoidal architecture in control and KO groups, whereas CCl_4-treated livers exhibited marked architectural distortion (Figure 5A). Histological analyses confirmed extensive fibrosis in the CCl_4 model and substantial lipid accumulation in the MCD and AFLD models (Figure 5C–D). Transporter expression analyses demonstrated heterogeneous regulation across models (Figure 6A–C). Oatp1b2 expression was markedly reduced in the KO group but increased in the CCl_4 model, whereas Mrp2 exhibited an opposing trend. Notably, transporter expression patterns did not parallel with MRI-derived functional measurements, suggesting dissociation between transporter abundance and effective hepatobiliary transport function.

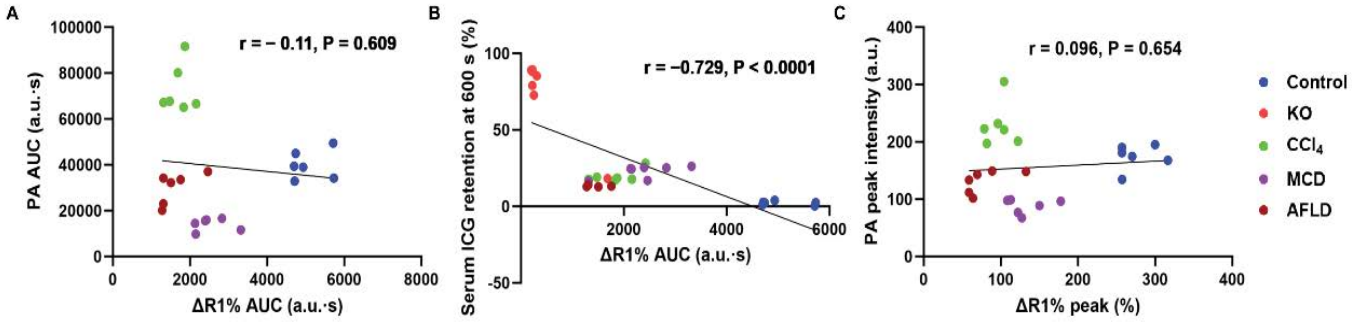

Figure 5: Correlation analyses between MRI-derived ΔR1% parameters, optoacoustic ICG metrics, and serum ICG retention.

A) Correlation between ΔR1% AUC and optoacoustic AUC ($r = -0.11$, $P = 0.609$, $n = 24$).

(B) Correlation between ΔR1% AUC and serum ICG retention at 600 s ($r = -0.729$, $P < 0.0001$, $n = 30$).

(C) Correlation between ΔR1% peak and optoacoustic peak intensity ($r = 0.096$, $P = 0.654$, $n = 24$).

The KO group was excluded from analyses involving optoacoustic parameters (A, C) because of negligible hepatic signal intensity. Data points are color-coded according to experimental group. Linear regression lines are shown for visualization purposes, and Spearman correlation coefficients (r) with corresponding P values are presented.

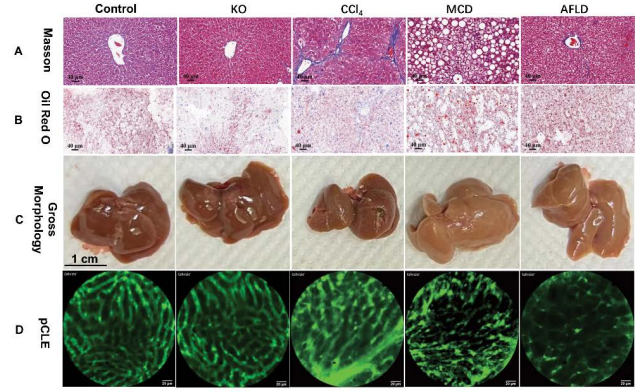

Figure 6: Histological and in vivo imaging validation of hepatocellular injury across experimental liver models.

(A) Representative in vivo probe-based confocal laser endomicroscopy (pCLE) images acquired 10 min after intravenous administration of 70 kDa FITC–dextran. Control and KO groups show preserved sinusoidal architecture, whereas CCl_4-treated livers exhibit distorted and thickened sinusoids; MCD livers display fragmented sinusoidal structures; AFLD livers show prominent signal-void regions.

(B) Representative gross liver morphology.

(C) Masson's trichrome staining showing collagen deposition (blue).

(D) Oil Red O staining showing hepatic lipid accumulation (red). Scale bars: (A) 20 μm; (B) 1 cm; (C, D) 40 μm.

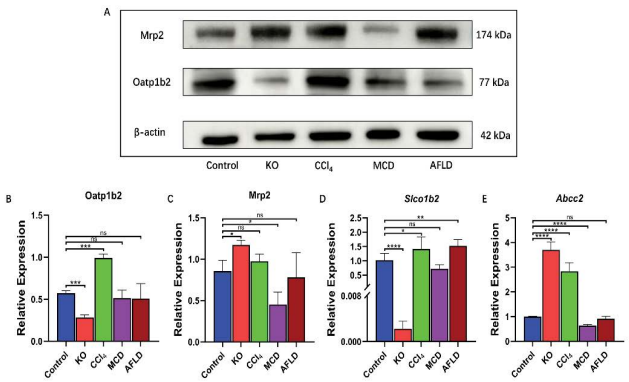

Figure 7: Hepatic expression of membrane transporters across experimental groups.

Citation: Yuting Zhu, Xun Hu, Zhuo Shi, Yuan Liang, Dengfeng Li, Peiqing Ma, Dong Yan, Jianwei Liang, Qian Wang. Gadoxetic Acid–Enhanced T1 Mapping Enables Transporter-Mediated Molecular Imaging of Liver Functional Reserve Journal of Radiology and Clinical Imaging. 9 (2026): 78-88.

(A) Representative Western blot images showing protein expression of organic anion–transporting polypeptide 1b2 (Oatp1b2) and multidrug resistance–associated protein 2 (Mrp2) in liver tissue. β-Actin was used as a loading control.

(B, C) Densitometric quantification of Oatp1b2 and Mrp2 normalized to β-actin (n = 3 per group).

(D, E) Relative mRNA expression levels of Slco1b2 and Abcc2 determined by quantitative real-time PCR (qRT-PCR) and normalized to the reference gene (n = 3 per group).

Data are presented as mean ± SD. Statistical analysis was performed using one-way ANOVA followed by post hoc multiple comparisons. *P < 0.05, **P < 0.01, ***P < 0.001, ****P < 0.0001 versus the control group.

Discussion

The present study demonstrates that ΔR1% derived from Gd-EOB-DTPA–enhanced T1 mapping provides a quantitative imaging biomarker capable of reflecting liver functional reserve across multiple mechanistically distinct liver injury models. Despite substantial heterogeneity in histopathology, transporter expression, and enhancement kinetics, ΔR1% consistently differentiated functional impairment severity and demonstrated a strong inverse association with systemic ICG retention. A major methodological implication of this work is the distinction between conventional signal intensity–based MRI assessment and quantitative parameter-based imaging. Traditional hepatobiliary MRI commonly relies on relative signal intensity measurements, which are highly influenced by scanner settings, acquisition parameters, and display windowing, thereby limiting reproducibility and inter-study comparability [33-37]. In contrast, quantitative T1 mapping provides a physically defined relaxation parameter that more directly reflects tissue contrast concentration and enables standardized longitudinal evaluation [38,39]. By expressing enhancement as ΔR1%, the present framework minimizes acquisition-dependent variability and improves quantitative comparability across experimental conditions. The longitudinal kinetic analyses further demonstrated distinct model-dependent hepatobiliary enhancement patterns. The transporter-deficient KO model showed nearly absent enhancement, whereas fibrosis and steatotic injury models exhibited intermediate yet separable enhancement behaviors. Importantly, all groups reached peak enhancement at approximately 10 min, suggesting that intergroup differences primarily reflected uptake magnitude and retention capacity rather than uptake timing alone. Cross-modality comparisons further clarified the physiological interpretation of the imaging findings. MRI-derived ΔR1% parameters did not significantly correlate with intrahepatic optoacoustic ICG kinetic parameters, despite both techniques interrogating hepatobiliary transport processes. This discrepancy likely reflects fundamental differences in imaging physics, probe behavior, and physiological sensitivity between MRI and optoacoustic imaging [40-43]. Gd-EOB-DTPA enhancement primarily reflects hepatocellular uptake and intracellular retention affecting tissue relaxation properties, whereas optoacoustic ICG imaging is additionally influenced by vascular distribution, optical attenuation, tissue scattering, and perfusion dynamics [44]. In contrast, ΔR1% AUC demonstrated a strong inverse relationship with systemic serum ICG retention, indicating that reduced hepatobiliary enhancement was closely associated with impaired whole-body clearance capacity. These findings support the interpretation that ΔR1% represents an integrated functional biomarker linking regional hepatocellular transport activity with organ-level clearance performance. At the molecular level, transporter expression patterns did not parallel imaging-derived functional measurements [45]. Oatp1b2 and Mrp2 expression exhibited heterogeneous regulation across injury models, yet these alterations were not consistently associated with ΔR1% or ICG-derived functional parameters. These findings suggest that transporter abundance alone is insufficient to determine effective hepatobiliary transport function. Several biological mechanisms may contribute to this dissociation. Effective hepatobiliary transport depends not only on transporter abundance but also on membrane localization, transporter activity, intracellular trafficking, substrate competition, perfusion efficiency, and microenvironmental integrity. In fibrotic and steatotic liver injury, architectural remodeling, sinusoidal distortion, lipid accumulation, and altered perfusion may substantially impair effective substrate delivery and biliary excretion independent of transporter transcriptional status [42,49,50]. This system-level interpretation is further supported by the marked pathological heterogeneity among liver injury models. The CCl_4 model was characterized by extensive fibrosis and architectural distortion, whereas the MCD and AFLD models predominantly exhibited steatosis and metabolic injury. Rather than reflecting isolated molecular pathways [46,47]. ΔR1% appears to integrate the combined physiological consequences of these complex pathological processes into a single quantitative parameter [41,48]. Several limitations should be acknowledged. First, transporter characterization was limited to expression-level analyses without direct assessment of membrane localization or transporter activity. Second, enhancement kinetics were summarized using simplified descriptors such as peak enhancement and AUC rather than formal pharmacokinetic compartment modeling [51]. Third, quantitative T1 mapping remains susceptible to respiratory motion and acquisition variability, emphasizing the need for rigorous protocol standardization. Finally, although the present study included diverse preclinical liver injury models, future clinical validation across different human disease etiologies and stages will be necessary. In conclusion, ΔR1% derived from Gd-EOB-DTPA–enhanced T1 mapping represents a quantitative imaging biomarker

capable of capturing integrated hepatobiliary functional performance across heterogeneous liver injury states. By linking hepatocellular transport behavior with systemic clearance capacity, this framework provides a mechanistically grounded and potentially translatable strategy for noninvasive assessment of liver functional reserve.

Funding Sources

This work was supported by the National Key Research and Development Program of China (2022YFB3203800), the National High-Level Hospital Clinical Research Funding (80102022505), the National Natural Science Foundation of China (92159305), and the Medical and Health Technology Innovation Project of the Chinese Academy of Medical Sciences (2023-I2M-2-004).

Conflict of Interest

The authors declare no competing financial interest.

Ethics Statement

All animal experiments were approved by the Ethics Committee for Laboratory Animals of the Cancer Hospital, Chinese Academy of Medical Sciences (Approval No. NCC2022A571) and were conducted in accordance with institutional and national guidelines.

Acknowledgement

The authors thank Peiqing Ma for valuable advice on pathological assessment.

Supplementary file Link:

https://cdn.fortunejournals.com/supply/gadoxetic-acid-ndash-enhanced-t1-mapping-enables-transporter-medi-10016-supplementary.docx

Reference

1. Hanahan D, Weinberg R A. Hallmarks of cancer: the next generation. Cell 144 (2011): 646-674.
2. Berasain C, Arechederra M,Argemí, et al. Loss of liver function in chronic liver disease: An identity crisis. J. Hepatol 78 (2023): 401-414.
3. Taru V, Szabo G, Mehal W, et al. Inflammasomes in chronic liver disease: Hepatic injury, fibrosis progression and systemic inflammation. J. Hepatol 81 (2024): 895-910.
4. Zhou I Y, Catalano O A, Caravan P. Advances in functional and molecular MRI technologies in chronic liver diseases. J. Hepatol 73 (2020): 1241-1254.
5. Schulze R J, Schott M B, Casey C A, et al. The cell biology of the hepatocyte: A membrane trafficking machine. J Cell Biol 218 (2019): 2096-2112.
6. Stieger B, Hagenbuch B. Recent advances in understanding hepatic drug transport. F1000Research 5 (2016): 2465.
7. D'Avola D, Granito A, Torre-Aláez M, et al. The importance of liver functional reserve in the non-surgical treatment of hepatocellular carcinoma. J. Hepatol 76 (2022): 1185-1198.
8. Tsubono T, Todo S, Jabbour N, et al. Indocyanine green elimination test in orthotopic liver recipients. Hepatology 24 (1996): 1165-1171.
9. Mahmut Z, Zhang C, Ruan F, et al. Medical Applications and Advancement of Near Infrared Photosensitive Indocyanine Green Molecules. Molecules 28 (2023).
10. Ba-Ssalamah A, Bastati N, Wibmer A, et al. Hepatic gadoxetic acid uptake as a measure of diffuse liver disease: Where are we? J. Magn. Reson. Imaging 45 (2017): 646-659.
11. Van de Steeg E, Wagenaar E, van der Kruijssen C M, et al. Organic anion transporting polypeptide 1a/1b-knockout mice provide insights into hepatic handling of bilirubin, bile acids, and drugs. J. Clin. Invest 120 (2010): 2942-2952.
12. Verloh N, Haimerl M, Zeman F, et al. Assessing liver function by liver enhancement during the hepatobiliary phase with Gd-EOB-DTPA-enhanced MRI at 3 Tesla. Eur. Radiol 24 (2014): 1013-1019.
13. Van Beers B E, Pastor C M, Hussain H K. Primovist, Eovist: what to expect? J. Hepatol 57 (2012): 421-429.
14. Zhao W, Zitzow J D, Weaver Y, et al. Organic Anion Transporting Polypeptides Contribute to the Disposition of Perfluoroalkyl Acids in Humans and Rats. Toxicol. Sci 156 (2017): 84-95.
15. Verloh N, Probst U, Utpatel K, et al. Influence of hepatic fibrosis and inflammation: Correlation between histopathological changes and Gd-EOB-DTPA-enhanced MR imaging. PLoS One 14 (2019): e0215752.
16. Utsunomiya T, Shimada M, Hanaoka J, et al. Possible utility of MRI using Gd-EOB-DTPA for estimating liver functional reserve. J. Gastroenterol 47 (2012): 470-476.
17. Yamada A, Hara T, Li F, Fujinaga Y, et al. Quantitative evaluation of liver function with use of gadoxetate disodium-enhanced MR imaging. Radiology 260 (2011): 727-733.
18. Watanabe H, Kanematsu M, Goshima S, et al. Staging hepatic fibrosis: comparison of gadoxetate disodium-enhanced and diffusion-weighted MR imaging--preliminary observations. Radiology 259 (2011): 142-150.
19. Verloh N, Rio Bartulos C, Utpatel K, et al. Volume-Assisted Estimation of Remnant Liver Function Based

on Gd-EOB-DTPA Enhanced MR Relaxometry: A Prospective Observational Trial. Diagnostics (Basel, Switzerland) 13 (2023).

20. Reimer P, Schneider G, Schima W. Hepatobiliary contrast agents for contrast-enhanced MRI of the liver: properties, clinical development and applications. Eur. Radiol 14 (2004): 559-578.
21. Kamimura K, Fukukura Y, Yoneyama T, et al. Quantitative evaluation of liver function with T1 relaxation time index on Gd-EOB-DTPA-enhanced MRI: comparison with signal intensity-based indices. J. Magn. Reson. Imaging 40 (2014): 884-889.
22. Dong Z, Wang M, Feng Y, et al. Feasibility of Imaging-Based Quantitative Hepatic Function Assessment: Gd-EOB-DTPA-Enhanced Liver MR Imaging Combined with T1 Mapping. Current medical imaging 19 (2023): 1394-1403.
23. Ding Y, Rao S X, Chen C, et al. Assessing liver function in patients with HBV-related HCC: a comparison of T_1 mapping on Gd-EOB-DTPA-enhanced MR imaging with DWI. Eur. Radiol 25 (2015): 1392-1398.
24. Messroghli D R, Moon J C, Ferreira V M, et al. Clinical recommendations for cardiovascular magnetic resonance mapping of T1, T2, T2* and extracellular volume: A consensus statement by the Society for Cardiovascular Magnetic Resonance (SCMR) endorsed by the European Association for Cardiovascular Imaging (EACVI). J. Cardiovasc. Magn. Reson 19 (2017): 75.
25. Zhang G, Li M, Feng H, et al. Hepatocyte uptake ratio derived from T1 mapping for quantitative assessment of liver fibrosis. Eur. Radiol (2025).
26. Haimerl M, Verloh N, Zeman F, et al. Gd-EOB-DTPA-enhanced MRI for evaluation of liver function: Comparison between signal-intensity-based indices and T1 relaxometry. Sci. Rep 7(2017): 43347.
27. Qu J, Han S, Zhang H, et al. Arterial Phase with CAIPIRINHA-Dixon-TWIST (CDT)-Volume-Interpolated Breath-Hold Examination (VIBE) in Detecting Hepatic Metastases. Transl. Oncol 10 (2017): 46-53.
28. Motosugi U, Ichikawa T, Sou H, et al. Liver parenchymal enhancement of hepatocyte-phase images in Gd-EOB-DTPA-enhanced MR imaging: which biological markers of the liver function affect the enhancement? J. Magn. Reson. Imaging 30 (2009): 1042-1046.
29. Feier D, Balassy C, Bastati N, et al. Liver fibrosis: histopathologic and biochemical influences on diagnostic efficacy of hepatobiliary contrast-enhanced MR imaging in staging. Radiology 269 (2013): 460-468.
30. Dostalek M, Sam W J, Paryani K R, et al. Diabetes mellitus reduces the clearance of atorvastatin lactone: results of a population pharmacokinetic analysis in renal transplant recipients and in vitro studies using human liver microsomes. Clin. Pharmacokinet 51 (2012): 591-606.
31. Shuboni-Mulligan D D, Parys M, Blanco-Fernandez B, et al. Dynamic Contrast-Enhanced MRI of OATP Dysfunction in Diabetes. Diabetes 68 (2019): 271-280.
32. Motosugi U, Ichikawa T, Sano K, et al. Double-Dose Gadoxetic Acid-Enhanced Magnetic Resonance Imaging in Patients With Chronic Liver Disease 46 (2011): 141-145.
33. Katsube T, Okada M, Kumano S, et al. Estimation of liver function using T1 mapping on Gd-EOB-DTPA-enhanced magnetic resonance imaging. Invest. Radiol 46 (4): 277-283.
34. Bataller R, Brenner D A. Liver fibrosis J Clin Invest 115 (2005): 209-218.
35. Rodríguez-Moreno F, González-Reimers E, Santolaria-Fernández F, et al. Zinc, copper, manganese, and iron in chronic alcoholic liver disease. Alcohol 14 (1997): 39-44.
36. Heye T, Yang S R, Bock M, et al. relaxometry of the liver: significant elevation of T1 relaxation time in patients with liver cirrhosis. Eur. Radiol 22 (2012): 1224-1232.
37. Oka H, Nakau K, Nakagawa S, et al. Liver T1/T2 values with cardiac MRI during respiration. Cardiol. Young 33 (2023): 1859-1865.
38. Sheagren C D, Cao T, Patel J H, et al. Motion-compensated T(1) mapping in cardiovascular magnetic resonance imaging: a technical review. Frontiers in cardiovascular medicine 10 (2023): 1160183.
39. Río Bártulos C, Senk K, Bade R, et al. Fully Automated Liver Function Score Calculated from Gd-EOB-DTPA-Enhanced MR Images: Diagnostic Performance vs. the MELD Score. Diagnostics (Basel, Switzerland) 12 (2022).
40. Sugiura R, Kuwatani M, Nishida M, et al. et al. Correlation between Liver Elasticity by Ultrasound Elastography and Liver Functional Reserve. Ultrasound Med Biol 45 (2019): 2704-2712.
41. Ma B, Xu H, Wu X, et al. Evaluation of liver function using Gd-EOB-DTPA-enhanced MRI with T1 mapping. BMC Med. Imaging 23 (2023): 73.
42. Wen X, Feng X, Kang Y, et al. Application Progress of Gd-EOB-DTPA-Enhanced MRI T1 Mapping in Hepatic Diffuse Diseases. Current medical imaging 18 (2022): 1276-1281.
43. Zhou Z P, Long L L, Qiu W J, et al. Evaluating segmental liver function using T1 mapping on Gd-EOB-DTPA-

enhanced MRI with a 3.0 Tesla. BMC Med. Imaging 17 (2017): 20.

44. Rassam F, Olthof P B, Bennink R J, et al. Current Modalities for the Assessment of Future Remnant Liver Function. Visceral medicine 33 (2017): 442-448.

45. Murray M, Zhou F. Trafficking and other regulatory mechanisms for organic anion transporting polypeptides and organic anion transporters that modulate cellular drug and xenobiotic influx and that are dysregulated in disease. Br J Pharmacol 174 (2017): 1908-1924.

46. Safatle-Ribeiro A V, Marques C F S, Pires C, et al. Diagnosis of Clinical Complete Response by Probe-Based Confocal Laser Endomicroscopy (pCLE) After Chemoradiation for Advanced Rectal Cancer. J. Gastrointest. Surg 25 (2021): 357-368.

47. Fuks D, Pierangelo A, Validire P, et al. Intraoperative confocal laser endomicroscopy for real-time in vivo tissue characterization during surgical procedures. Surg. Endosc 33 (2019): 1544-1552.

48. Wang Q, Kesen S, Liljeroth M, et al. Quantitative evaluation of liver function with gadoxetic acid enhanced MRI: Comparison among signal intensity-, T1-relaxometry-, and dynamic-hepatocyte-specific-contrast-enhanced MRI- derived parameters. Scand. J. Gastroenterol 57 (2022): 705-712.

49. Pan Q, Zhu G, Xu Z, et al. Organic Anion Transporting Polypeptide (OATP) 1B3 is a Significant Transporter for Hepatic Uptake of Conjugated Bile Acids in Humans. Cell. Mol. Gastroenterol. Hepatol 16 (2023): 223-242.

50. Ma X, Shang X, Qin X, et al. Characterization of organic anion transporting polypeptide 1b2 knockout rats generated by CRISPR/Cas9: a novel model for drug transport and hyperbilirubinemia disease. Acta pharmaceutica Sinica. B 10 (2020): 850-860.

51. Xu R, Yu D, Luo P, et al. Do Habitat MRI and Fractal Analysis Help Distinguish Triple-Negative Breast Cancer From Non-Triple-Negative Breast Carcinoma. Can. Assoc. Radiol. J 75 (2024): 584-592.

Citation: Yuting Zhu, Xun Hu, Zhuo Shi, Yuan Liang, Dengfeng Li, Peiqing Ma, Dong Yan, Jianwei Liang, Qian Wang. Gadoxetic Acid–Enhanced T1 Mapping Enables Transporter-Mediated Molecular Imaging of Liver Functional Reserve Journal of Radiology and Clinical Imaging. 9 (2026): 78-88.